https://doi.org/10.5194/egusphere-2026-6561
Preprint. Discussion started: 5 November 2026
© Author(s) 2026. CC BY 4.0 License.

From Sub-Diffusion to Fickian Diffusion of Conservative Solute Tracers in Porous Rocks

Tingchang Yin[1] and Brian Berkowitz[1]

[1]Department of Earth and Planetary Sciences, Weizmann Institute of Science, Rehovot 7610001, Israel

Correspondence: Tingchang Yin (tingchang.yin@weizmann.ac.il)

Abstract. Molecular diffusion of conservative solute tracers is relevant to many hydrogeological scenarios, such as contaminant and radionuclide migration. Sub-diffusion—wherein the mean squared displacement grows sub-linearly with time due to prolonged trapping in the pore space—can occur in porous rocks but is expected to evolve asymptotically toward Fickian diffusion at long times. However, this transition has received little attention in the literature. Here, simulations of diffusion are conducted using particle-tracking methods in three digital porous-rock domains. The first two rocks are extracted from real rock samples, and periodic boundary conditions are imposed on both of them. The third rock is constructed by combining several rock samples and is therefore a long, artificial, and highly heterogeneous rock column. The survival probability computed from the simulations demonstrates clearly the transition from sub-diffusion to Fickian diffusion. We then derive an analytical survival probability model within the continuous time random walk (CTRW) framework; a truncated waiting-time distribution is used to introduce a finite characteristic time scale. For the first two rocks, the transition can be captured by the CTRW model, whereas the Fickian model is inadequate, when the observation time is comparable to or exceeds the finite time scale. For the third rock, neither the CTRW nor the Fickian model can adequately describe the transition due to its strongly heterogeneous nature. The implications of sub-diffusion are illustrated through an example in which a diffusive tracer plume arrives much earlier than predicted by the Fickian model. Both the numerical results and the analytical model highlight the importance of properly accounting for sub-diffusion in diffusion modeling of porous rocks.

1 Introduction

In subsurface porous rocks, the transport of solute tracers is driven mainly by molecular diffusion (Fetter et al., 2017, pp. 58–61) when advection is absent. Diffusive solute transport occurs in a variety of scenarios, including contaminant migration in low-permeability clays and crystalline rocks (Delay et al., 2002; Dentz et al., 2012) and radionuclide transport in deep geological repositories for nuclear waste disposal (Soler et al., 2022). Although diffusion generally transports solute chemicals very slowly (compared to subsurface flow), it plays a critical role in the long-term safety assessment of underground repositories (Wersin et al., 2004), as it governs the migration of contaminants over geological timescales.

Molecular diffusion in subsurface porous rocks is generally assumed to be Fickian (Gouze et al., 2008; Tartakovsky and Dentz, 2019). This assumption has been adopted widely in both experimental (García-Gutiérrez et al., 2006; Garcia-Gutierrez

https://doi.org/10.5194/egusphere-2026-6561
Preprint. Discussion started: 5 November 2026
© Author(s) 2026. CC BY 4.0 License.

et al., 2023) and numerical (Nasir et al., 2014; Grigaliuniene et al., 2024) studies, where an effective diffusion coefficient is used to characterize the bulk diffusive behavior.

However, the Fickian assumption may not always be valid. Recent diffusion experiments (Rajyaguru et al., 2024, 2025) in porous rocks (lasting approximately 70 days) have revealed noticeable early arrivals and late-time tails in breakthrough curves, indicating sub-diffusion (wherein their mean-squared displacement grows sub-linearly with time due to prolonged trapping in the pore space) that cannot be captured by Fickian models. To explore the origin of sub-diffusion, particle-tracking simulations of tracer diffusion in porous rocks have been conducted (Yin and Berkowitz, 2026) to show that the trapping effect of low-connectivity zones within the domain leads to heavy late-time tails.

A transition from sub-diffusion to Fickian diffusion in general porous media is expected when the observation length or time scale is sufficiently large and the correlation length governing diffusion is finite (Koch and Brady, 1988; Regner et al., 2013), although for geological media, the existence of a finite correlation length may at least in some cases be questionable (Berkowitz, 2021). Moreover, in terms of percolation theory (Stauffer and Aharony, 2018), which is sometimes considered applicable to natural porous media and describes poorly connected networks spanning the domain with large "dead-end" clusters attached, the correlation length can become infinitely large near the percolation threshold (Sahimi, 2011, p. 27). Note that many previous studies (Dentz et al., 2004; Berkowitz and Scher, 2009; Bijeljic et al., 2011; Deng et al., 2025; Cohen and Berkowitz, 2026) have demonstrated the transition from non-Fickian dispersion to Fickian transport in geological media under disordered velocity fields and/or chemical reactions. Here, we focus solely on diffusion without additional drifts.

Diffusion experiments (Zhokh and Strizhak, 2019) and simulations (Aarão Reis and Di Caprio, 2014) in artificial porous materials have demonstrated such transitions and shown that the classical Fickian model is insufficient to describe the temporal evolution of diffusion. However, no study has focused on the transition to Fickian diffusion in natural porous rocks, which generally exhibit much stronger heterogeneity than artificial porous materials.

To address these considerations, the transition from sub-diffusion to Fickian diffusion in porous rocks is investigated using both analytical models and numerical simulations. We perform particle-tracking simulations to reproduce the transition behavior in three-dimensional (3D) digital rock samples. Generally, the sizes of CT-scanned rock samples are limited, which may prevent the transition to Fickian diffusion from being observed within them. In this study, periodic boundary conditions are imposed on the generated digital rocks in the x direction, allowing solute tracers to diffuse over sufficiently long times and distances. Such boundary conditions are widely adopted in porous media flow and transport simulations (Clarke et al., 2021; Wu et al., 2024; Arbabi and Sahimi, 2024), under the assumption that solute tracers experience similar porous structure repeatedly over long times.

We then introduce a continuous time random walk (CTRW) model with a truncated waiting-time distribution to derive an analytical model for the survival probability of conservative solute tracers in finite domains; the survival probability represents the complementary cumulative distribution function of the first-passage time. Combining the survival probability model with the numerical simulations, we aim to reproduce and elucidate both the early-time sub-diffusion and the asymptotic Fickian diffusion observed at long times.

https://doi.org/10.5194/egusphere-2026-6561
Preprint. Discussion started: 5 November 2026
© Author(s) 2026. CC BY 4.0 License.

This paper is organized as follows. In Section 2, we present the generation of digital porous rocks and the particle-tracking method, including the boundary conditions, initial conditions, and control-plane pairs (used to obtain first-passage times over finite distances). We also introduce the two observables computed from the numerical simulations, together with the CTRW model and the derivation of the corresponding analytical survival probability model. In Section 3, we demonstrate the transition from sub-diffusion to Fickian diffusion using both the analytical model and the numerical results. The role of the finite characteristic time scale is discussed, and the computed survival probability curves are fitted using the analytical model. The implications of sub-diffusion are also discussed. Finally, concluding remarks are provided in Section 4.

2 Methods

We first present the generated porous media, the numerical setup for the diffusion simulations, and the definitions of the computed observables. We then introduce the truncated CTRW model and derive the corresponding survival probability model. For comparison, the Fickian survival probability model is also presented.

2.1 Numerical simulations

2.1.1 Digital porous media

The CT scan data of rocks (Vidal et al., 2024; Eduardo Menezes dos Anjos et al., 2024) are used to generate voxelized porous media. Only the spanning cluster (i.e., the connected pore voxels spanning the domain in the x direction) is retained. In this subsection, the domain sizes and pore sizes are expressed only in terms of the number of voxels. The corresponding physical domain dimensions L_m and voxel sizes l_v of the generated porous media are presented in Section 2.1.4.

The pore structure of real rocks is heterogeneous. To eliminate structural bias between the two sides of the initial condition, mirror symmetrization is used to construct the porous media. Specifically, the original voxelized porous medium is reflected in the x direction to generate its mirror image. The original medium and its mirror image are then concatenated along the x direction to produce a mirror-symmetric porous medium. The initial condition is located on the central plane of the mirror-symmetric medium, as discussed in Section 2.1.3. This construction ensures that the diffusion plume encounters statistically identical pore structures on both sides of its initial location, thereby preventing apparent differences in diffusion rates caused solely by structural asymmetry.

The three media are shown in Figure 1. The first two porous media are generated from the rock samples SW04 and P04 (Vidal et al., 2024), respectively. Their dimensions are $388 \times 173 \times 144$ and $406 \times 156 \times 158$ voxels, respectively, with mean pore diameters of 4.326 and 4.738 voxels. The corresponding effective porosities are 11.14% and 8.74%, respectively.

The third porous medium, denoted by P^{C} in this study, is significantly longer in the x direction and is constructed from six rock samples (P01–P06; see Vidal et al., 2024, Table 1). The samples are concatenated with an overlap of 40 voxels in the x direction because the pore connectivity is generally discontinuous across the boundaries of different samples. Within each overlapping region, a voxel is classified as pore space if it belongs to the pore phase in either sample. The resulting

https://doi.org/10.5194/egusphere-2026-6561
Preprint. Discussion started: 5 November 2026
© Author(s) 2026. CC BY 4.0 License.

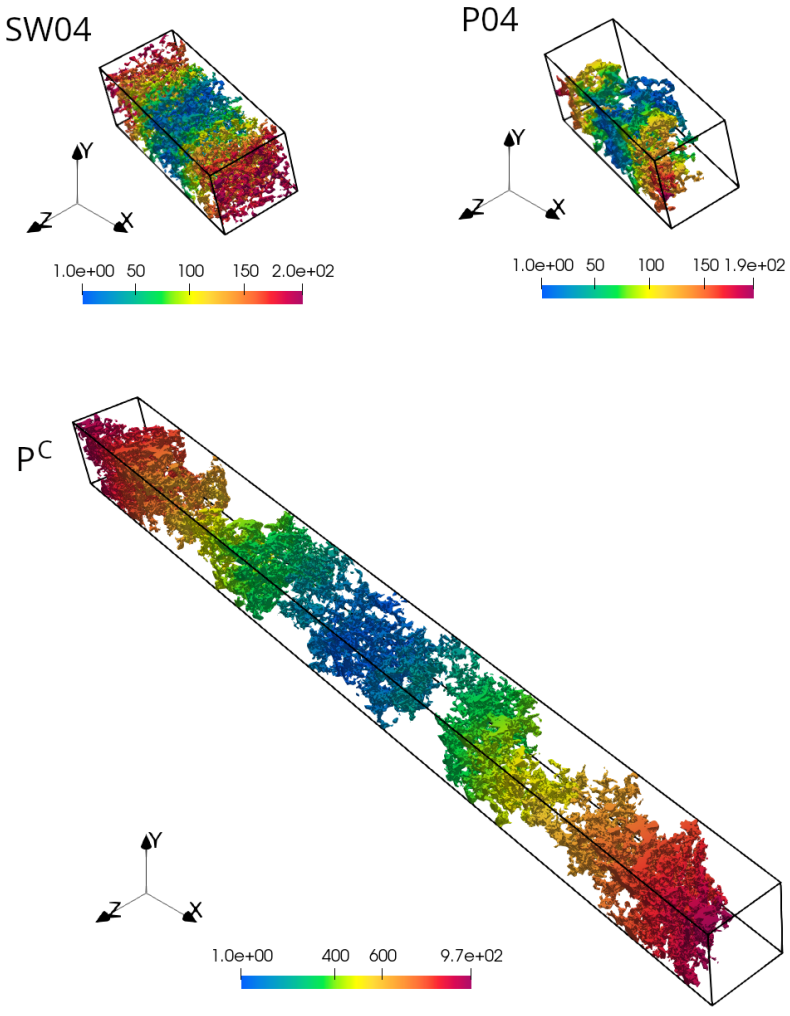


Figure 1. The three generated porous media: SW04, P04, and P^C. The colors denote the distance of the voxels from the central plane. The physical domain sizes of all three rocks are rescaled to 1 cm, as discussed in Section 2.1.4.

concatenated porous medium is subsequently mirror-symmetrized, as shown at the bottom of Figure 1. Its dimensions are $1946 \times 153 \times 144$ voxels, with a mean pore diameter of 4.978 voxels and an effective porosity of 9.19%. Although this porous medium is artificially constructed, it provides a representative example of a highly heterogeneous rock column over a relatively long length scale.

2.1.2 Characteristics of the three porous media

The first two porous media investigated in this study are generated from individual rock samples, as described in Section 2.1.1. The sample P04 is less space-filling and has lower porosity, whereas the sample SW04 is more space-filling and has higher

https://doi.org/10.5194/egusphere-2026-6561
Preprint. Discussion started: 5 November 2026
© Author(s) 2026. CC BY 4.0 License.

porosity. Particle-tracking simulations with periodic boundary conditions (as shown in Section 2.1.3) are performed in these two media to investigate how long it takes for the possible transition to Fickian diffusion to occur while allowing particles to repeatedly experience the same pore structures under lower/higher porosity.

The third porous medium $\mathrm{P^C}$ is constructed based on a different consideration. Because periodic boundary conditions are not generally realistic, a relatively long rock column is created by concatenating multiple rock samples to complement the investigation of the transition to Fickian diffusion over sufficiently long distances. In this case, the control planes (used to compute survival probability curves at different length scales) are placed only within the interval $[0, L_m]$, as discussed in Section 2.1.3.

2.1.3 Particle-tracking methods

Discrete-time scheme. Diffusion in voxelized porous structures is simulated using the Lagrangian discrete-time particle-tracking method (Zhang et al., 2022; Yin et al., 2024, 2025):

$$\Delta \boldsymbol{x} = \boldsymbol{\xi}\sqrt{2D_m \Delta t}, \tag{1}$$

where $\Delta \boldsymbol{x} \in \mathbb{R}^3$ is the particle displacement during each time step, Δt is the time-step size, $\boldsymbol{\xi}$ is a vector of independent standard normal random variables, and D_m is the pore-scale molecular diffusion coefficient.

Initial conditions. The initial condition (light green plane in Figure 2) is located at the central plane ($x = L_m/2$) of the domain. Lagrangian tracer particles are initially released from this plane and subsequently diffuse toward both sides of the domain.

Boundary conditions. Periodic boundary conditions (light red planes in Figure 2) are imposed on the two opposite faces in the x direction. Under periodic boundary conditions, a particle crossing the boundary at $x = 0$ or $x = L_m$ is reintroduced at the opposite side of the domain. The mirror-symmetric construction ensures that the pore spaces match across the two opposite faces. Reflection boundary conditions are imposed on all other faces and pore walls to ensure a locally uniform particle distribution (Szymczak and Ladd, 2003).

Control planes. Multiple pairs of control planes (light blue planes in Figure 2) are placed within the domain to detect particle crossings. Survival probability curves are then computed for different pairs of control planes, as discussed in Section 2.1.5. Owing to the periodic boundary conditions, control planes may also be positioned at locations with x coordinates outside the interval $[0, L_m]$, except the sample $\mathrm{P^C}$.

2.1.4 Simulation parameters

The simulation parameters used in this study are summarized below. Unless otherwise specified, the length and time units are centimeters (cm) and seconds (s), respectively.

- **Domain size** (L_m): For all generated porous media, the domain length in the x-direction is normalized to $L_m = 1$ cm, while the domain dimensions in the other directions are scaled proportionally. This choice is reasonable because, for example, the voxel size l_v of sample $\mathrm{P^C}$ is $1/1946 \approx 5.14 \times 10^{-4}$ cm, corresponding to a mean pore diameter of approx-

https://doi.org/10.5194/egusphere-2026-6561
Preprint. Discussion started: 5 November 2026
© Author(s) 2026. CC BY 4.0 License.

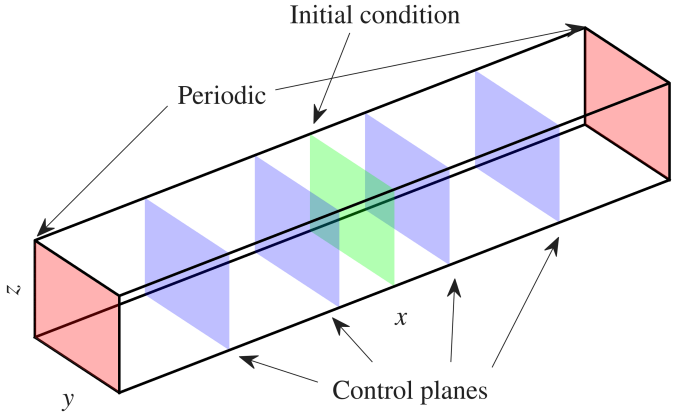


Figure 2. Illustration of the initial condition, control planes, and boundary conditions.

imately five voxels, or 0.0026 cm (26 μm). This value falls within the typical pore-size range of carbonate rocks (Sowiżdżał et al., 2022).

- **Molecular diffusion coefficient** (D_m): The molecular diffusion coefficient is set to $D_m = 1 \times 10^{-5}$ cm^2/s, which is consistent with the order of magnitude of diffusion coefficients for common chemical tracers in water.
- **Time-step size** (Δt): The time-step size is chosen to be approximately one order of magnitude smaller than l_v^2/D_m.
- **Number of tracer particles** (N_p): The number of tracer particles is set to $N_p = 1 \times 10^4$.
- **Location of control-plane pairs** (l_c): The location of a control-plane pair is specified by its distance from the central plane. For example, $l_c = 0.2$ cm indicates that the two control planes are located at $x = L_m/2 \pm 0.2$ cm. We set five control-plane pairs in each rock: $(0.4, 0.5, 1.0, 1.5, 2.0)$ cm for SW04, $(1.0, 2.0, 3.0, 4.0, 5.0)$ cm for P04, and $(0.1, 0.2, 0.3, 0.4, 0.5)$ cm for P$^{\mathrm{C}}$. As $L_m = 1$ cm, a control-plane pair with $l_c = 2$ cm means that the first-passage times of particles are measured at locations where the particles have already crossed two repeated domains in either the negative or positive x direction.

2.1.5 Computed observables

Based on the simulation results, two observables are computed: the mean squared displacement (MSD) (Pacheco-Pozo and Sokolov, 2023), which quantifies how far tracer particles move from their initial positions over time, and the survival probability (Redner, 2023), which characterizes the retention behavior over time at a given length scale. These two observables not only distinguish Fickian diffusion from sub-diffusion but also reveal the transition between them over different time/length scales, as described below.

https://doi.org/10.5194/egusphere-2026-6561
Preprint. Discussion started: 5 November 2026
© Author(s) 2026. CC BY 4.0 License.

Mean squared displacements. The MSD is calculated as

$$\mathrm{MSD}(t) = \frac{1}{N_p}\sum_{i=1}^{N_p}[x_i(t) - x_i(0)]^2, \tag{2}$$

where $x_i(t)$ denotes the x coordinate of the ith particle at time t. The domain for numerical simulations is 3D, and only the projection of particle displacement onto the x direction is considered when calculating the MSD. The same applies to the survival probability defined below.

For Fickian diffusion, the MSD is linearly proportional to t. When

$$\mathrm{MSD}(t) \sim t^{\beta},$$

where β is the MSD exponent, diffusion is non-Fickian if $\beta \neq 1$. In particular, sub-diffusion is characterized by $0 < \beta < 1$. The MSD curves are computed throughout the simulations to identify Fickian and non-Fickian diffusion.

Survival probability. For each pair of control planes, the first-passage time, denoted by t_f, at which a particle first reaches either control plane is recorded. The survival probability is then computed as

$$S^N(t) = \frac{N(t_f > t)}{N_p}, \tag{3}$$

where the superscript N indicates that the survival probability is obtained from numerical simulations, and $N(t_f > t)$ denotes the number of particles whose first-passage times exceed t for the given pair of control planes.

2.2 Truncated CTRW

The CTRW is a stochastic framework for describing both Fickian and non-Fickian diffusion. Within this framework, the diffusion process is classically represented by the Montroll–Weiss equation (Montroll and Weiss, 1965; Metzler et al., 2022) in Fourier–Laplace space, whose long-time and large-scale limit yields continuum diffusion equations. In this work, we employ an equivalent integro-differential formulation (Fa and Wang, 2010) in physical space and time, which was shown to be well suited for finite-domain problems. The one-dimensional (1D) governing equation is given by

$$\frac{\partial C(x,t)}{\partial t} = \int_0^t g(t-t_1)\frac{\partial C(x,t_1)}{\partial t_1}\mathrm{d}t_1 + D\frac{\partial}{\partial t}\int_0^t g(t-t_1)\frac{\partial^2 C(x,t_1)}{\partial x^2}\mathrm{d}t_1, \tag{4}$$

where $C(x,t)$ is the concentration profile, and $g(t)$ is the prescribed waiting-time probability density function (PDF). Note that Equation (4) assumes a Gaussian jump-length PDF, with $D = \sigma^2/2$, where σ is the standard deviation of the jump-length distribution.

Here, we adopt a truncated waiting-time PDF (Fa, 2010), given by

$$g(t) = \frac{b^\alpha}{\Gamma(\alpha)}t^{\alpha-1}\exp(-bt), \tag{5}$$

where $\alpha > 0$ controls the strength of non-Fickian diffusion, $b > 0$ determines how long the non-Fickian behavior persists, and $\Gamma(\cdot)$ denotes the Gamma function. A smaller α value generally indicates stronger transient sub-diffusive behavior. A larger b

https://doi.org/10.5194/egusphere-2026-6561
Preprint. Discussion started: 5 November 2026
© Author(s) 2026. CC BY 4.0 License.

value generally results in a shorter range of power-law behavior. From a long-time perspective, b has the most significant effect, as it largely determines t_m and controls the onset of the transition.

We choose this waiting-time PDF because it can describe transient sub-diffusion followed by asymptotic Fickian diffusion. To explain this, we show that such a PDF is characterized by a finite time scale,

$$t_m = \frac{\alpha}{b}, \tag{6}$$

which approximately marks the transition from the initial power-law waiting-time behavior to the exponentially truncated regime. Note that t_m does not represent an exact transition time at which the exponential term begins to dominate in Equation (5); rather, there is no mathematically sharp point at which this dominance begins. In the time regimes $t \ll t_m$ and $t \gg t_m$, the power-law behavior and exponential truncation dominate, respectively. Consequently, the diffusion progressively approaches the Fickian limit for $t \gg t_m$.

Substituting Equation (5) into Equation (4), the exact solution for the concentration profile (Fa, 2010) can be obtained:

$$C(x,t) = \frac{1}{2\pi\sqrt{Db^\alpha}} \int_0^\infty \Phi(\omega,x)\cos[\omega t + \theta(\omega,x)]\,\mathrm{d}\omega, \tag{7}$$

where $\Phi(\omega,x)$ and $\theta(\omega,x)$ are auxiliary functions, whose definitions are provided in Appendix A. The unit of $C(x,t)$ is length to the power of -1, as the amount of substance is treated as dimensionless in the particle-tracking simulations. Note that Equation (7) is Green-function-like and exhibits translation invariance.

We consider a finite 1D domain spanning $0 \le x \le L$ with absorbing boundary conditions at both ends. The initial condition is a Dirac delta function located at $x = L/2$. The exact solution for the concentration profile in the finite domain, denoted by $C_A(x,t)$, can then be constructed using the method of images (Metzler and Klafter, 2000) as

$$C_A(x,t) = \sum_{n=-\infty}^{\infty} \left[C\left(x - \left(2nL + \frac{L}{2}\right), t\right) - C\left(x - \left(2nL - \frac{L}{2}\right), t\right)\right]. \tag{8}$$

The survival probability, which represents the normalized "amount" of solute tracer particles remaining within the 1D domain, is obtained from the truncated CTRW model (Equation (8)) by integrating the concentration profile over the finite domain,

$$S(t) = \int_0^L C_A(x,t)\,\mathrm{d}x, \tag{9}$$

which yields

$$S(t) = \frac{1}{2\pi\sqrt{Db^\alpha}} \int_0^\infty A(\omega)\left[\left(\mathcal{I}_c^{(+)} - \mathcal{I}_c^{(-)}\right)\cos(\omega t + \phi(\omega)) + \left(\mathcal{I}_s^{(+)} - \mathcal{I}_s^{(-)}\right)\sin(\omega t + \phi(\omega))\right]\mathrm{d}\omega, \tag{10}$$

where $A(\omega)$, $\mathcal{I}_c^{(+)}$, $\mathcal{I}_c^{(-)}$, $\mathcal{I}_s^{(+)}$, $\mathcal{I}_s^{(-)}$, and $\phi(\omega)$ are auxiliary functions defined in Appendix B. The oscillatory integral with respect to ω generally admits no closed-form solution. Therefore, $S(t)$ is evaluated numerically using the Levin method (Chen et al., 2024).

https://doi.org/10.5194/egusphere-2026-6561
Preprint. Discussion started: 5 November 2026
© Author(s) 2026. CC BY 4.0 License.

As a comparison, we introduce the Fickian survival probability model (Redner, 2001), denoted by $S_f(t)$, which is given by

$$S_f(t) = \int_{-a}^{a} \sum_{m=0}^{\infty} (-1)^m G(x,t,D_e;2am)\,\mathrm{d}x, \tag{11}$$

where $a = L/2$, $G(x,t,D_e;x_0) = (4\pi D_e t)^{-1}\exp\left[-(x-x_0)^2/(4D_e t)\right]$ is the Green's function, x_0 denotes the location of the initial condition, and D_e is the 1D effective Fickian diffusion coefficient. Note that the integration domain in Equation (11) is shifted from $[0, L]$ to $[-a, a]$, which does not affect the validity of the solution.

3 Results and Discussion

We first compare the analytical survival probability curves determined by the CTRW and Fickian models, i.e., $S(t)$ and $S_f(t)$, respectively, to demonstrate the analytical transition from sub-diffusion to Fickian diffusion controlled by the characteristic time scale t_m. We then present the numerical survival probability curves, $S^N(t)$, computed from particle-tracking simulations in the three porous rocks. The analytical models $S(t)$ and $S_f(t)$ are fitted to the computed $S^N(t)$ curves under different control-plane pairs to elucidate the transition using both analytical and numerical evidence. Finally, the implications of early-time sub-diffusion are discussed.

3.1 Transitions shown by analytical models

The truncated CTRW framework presented in Section 2.2 is controlled by a finite characteristic time scale, t_m. Within this framework, diffusion transitions from non-Fickian to Fickian behavior when the observation time scale is much larger than t_m. To demonstrate this transition from the perspective of survival probability, two sets of parameters are used to generate the CTRW-based survival probabilities $S(t)$ (Equation (10)), which are then compared to the Fickian model $S_f(t)$ given by Equation (11). The two parameter sets for the CTRW model are shown in Table 1. The main difference between them is the value of b, which results in substantially different t_m values and is used to demonstrate the adaptability of the model. The other parameters are also changed to introduce additional variability.

Table 1. Parameter sets used to generate the CTRW-based survival probabilities.

Parameter set	D	α	b	t_m
1	1	0.5	0.2	0.5
2	1×10^{-6}	0.8	1×10^{-5}	8×10^{4}

The generated $S(t)$ curves are shown in Figure 3. The $S(t)$ curves are fitted using the Fickian model $S_f(t)$ through the non-linear least-squares method, and the fitted parameters are shown in Table 2. The role of the characteristic time scale t_m (Equation (6)) is clearly illustrated in both subplots. Although the two parameter sets differ by several orders of magnitude and indicate survival probability curves over substantially different time scales under different domain sizes L, they exhibit the same qualitative behavior. Before t_m, the $S(t)$ curves deviate markedly from the Fickian model $S_f(t)$ as shown in Figure 3,

https://doi.org/10.5194/egusphere-2026-6561
Preprint. Discussion started: 5 November 2026
© Author(s) 2026. CC BY 4.0 License.

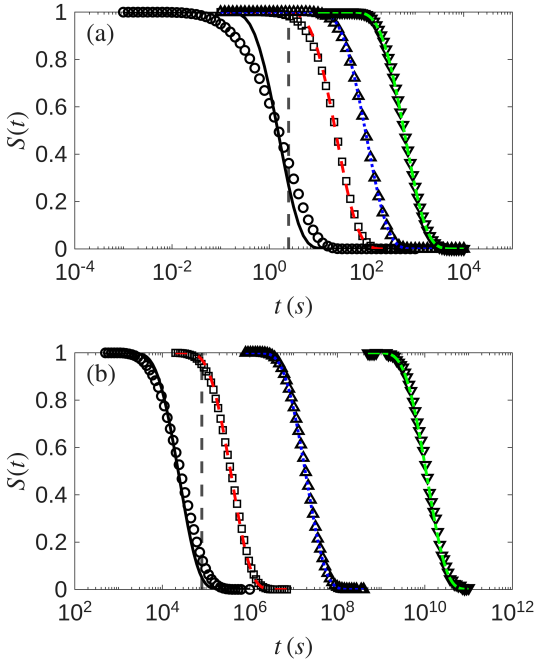


Figure 3. Generated $S(t)$ curves (hollow markers) and their best fits using the Fickian model $S_f(t)$ (curves). (a) Parameter set 1. (b) Parameter set 2. The vertical dashed lines denote the t_m values (Equation (6)), with $t_m = 2.5$ s in (a) and $t_m = 80000$ s in (b). The L values (denoted by different markers in both (a) and (b)), the effective Fickian diffusion coefficients D_e, and the coefficients of determination R^2, which quantify the goodness of fit of the Fickian model, are shown in Table 2.

exhibiting pronounced early arrivals and late-time tails. After t_m, the $S(t)$ curves gradually approach Fickian behavior, as evidenced by the increasing coefficients of determination R^2 (Table 2). Also, the fitted D_e values become constant at large L values.

Again, from a mathematical viewpoint, the characteristic time scale t_m does not represent the exact transition time from sub-diffusion to Fickian diffusion; however, it can serve as a reference time scale for this transition. In Figure 3, when the $S(t)$ curves begin to decay from one at times smaller than or only slightly larger than t_m (e.g., the curves represented by hollow square markers in both Figure 3a and b), sub-diffusive behavior is still evident, as indicated by the relatively low R^2 values shown in Table 2. When $S(t)$ begins to decay from one at a time much larger than t_m (approximately two orders of magnitude larger in Figure 3), the diffusion can be well described by the Fickian model.

The characteristic time scale can be interpreted as a characteristic length scale, $l_m = \sqrt{D_e t_m}$, where D_e should be the effective diffusion coefficient fitted in the Fickian regime using Equation (11). The corresponding l_m values are approximately 1 cm and 0.001 cm for the two parameter sets, respectively. From Figure 3, it can be seen that when $L \gg l_m$, diffusion is Fickian.

https://doi.org/10.5194/egusphere-2026-6561
Preprint. Discussion started: 5 November 2026
© Author(s) 2026. CC BY 4.0 License.

Table 2. The L values, the effective diffusion coefficients D_e, and the coefficients of determination R^2 obtained from the best fits using the Fickian model $S_f(t)$ in Figure 3a and b.

	(a): Parameter set 1			(b): Parameter set 2		
Marker	L	D_e	R^2	L	D_e	R^2
○	3	5.69×10^{-1}	0.9823	0.002	1.64×10^{-11}	0.9904
□	10	4.14×10^{-1}	0.9991	0.0007	1.28×10^{-11}	0.9992
△	20	4.01×10^{-1}	0.9999	0.05	1.28×10^{-11}	0.9998
▽	50	4.01×10^{-1}	1	1.2	1.28×10^{-11}	0.9994

Note that the choice of the waiting-time distribution, Equation (5), makes the resulting survival probability solution in Equation (11) inapplicable to pure sub-diffusion without transition. For sufficiently small but finite values of b, the value of t_m becomes very large, indicating that a transition still exists, e.g., the parameter set 2 (Table 1). However, if $b = 0$, the waiting-time distribution becomes meaningless because the factor b^α vanishes, even though $\exp(-bt) = 1$. Such a choice is only suitable for finite domains with finite trapping times for tracer particles. Therefore, decreasing b does not eliminate the Fickian regime but instead postpones its onset to increasingly longer times. For infinitely long trapping times, the time-fractional diffusion equation provides a suitable alternative (Metzler and Klafter, 2000; Metzler et al., 2022; Rajyaguru et al., 2025).

3.2 Analyses of numerical results

3.2.1 Mean squared displacement and transition times

The computed MSD curves for diffusion in the three porous media are shown in Figure 4. At early times, all the MSD curves exhibit sub-linear behavior, with $\beta < 1$. The MSD curves enter the asymptotic Fickian diffusion regime, and with $\beta \to 1$ at later times.

For SW04, which has relatively high porosity and is more space-filling, the transition to Fickian diffusion is very smooth (Figure 4a). For the other two samples, noticeable variations can be observed in the MSD curves, i.e., the diffusion rates do not increase monotonically. The heterogeneous structures within P04 and $\mathrm{P^C}$ can repeatedly trap and release tracer particles, causing the bulk diffusion rate to fluctuate. This phenomenon is particularly pronounced in the MSD curve of $\mathrm{P^C}$, as it is an artificial porous medium constructed by concatenating different rock samples with overlapping regions.

The characteristic times t_m can be estimated roughly from the MSD curves by identifying the transition from sub-diffusion to Fickian diffusion, as indicated by the black dashed vertical lines in Figure 4. The estimated t_m values are equal to the ratios of α to b listed in Table 3, which are then used to fit the computed survival probabilities in Section 3.2.2.

https://doi.org/10.5194/egusphere-2026-6561
Preprint. Discussion started: 5 November 2026
© Author(s) 2026. CC BY 4.0 License.

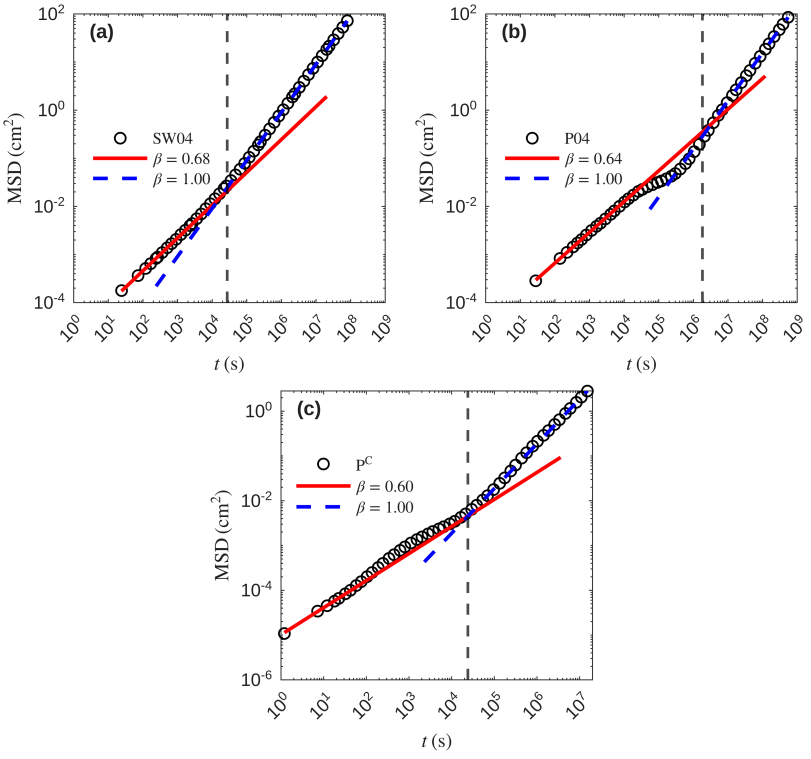


Figure 4. MSD curves for the three porous media. (a) SW04; (b) P04; and (c) $\mathrm{P^C}$. The red solid and blue dashed lines in each subplot serve as references for the β values at early and late times, respectively. The black vertical dashed lines denote the t_m values, which are roughly estimated from the transition times from sub-diffusion to Fickian diffusion observed in the MSD curves.

3.2.2 Survival probability analyses

Control-plane pairs with different l_c values are specified during the simulations, and the corresponding survival probability curves, $S^N(t)$, are computed, as shown in Figure 5. The truncated CTRW model $S(t)$ and Fickian $S_f(t)$ are then fitted to the computed $S^N(t)$ curves, respectively. When fitting $S(t)$, appropriate values of α and b are chosen such that t_m (Equation (6)) matches the estimated characteristic times discussed in the previous subsection, which are also indicated by the dashed black vertical lines in Figure 5; the α values are chosen to be equal to the early-time β values shown in Figure 4, because early time diffusion is characterized by a power law waiting time PDF. The L values are equal to $2l_c$, which also denotes the number of repeated domains that solute tracers have experienced under periodic boundary conditions for samples SW04 and P04. Note that although the physical domain size L_m of all three rocks is rescaled to 1 cm, their dimensions are $388 \times 173 \times 144$ voxels (SW04), $406 \times 156 \times 158$ voxels (P04), and $1946 \times 153 \times 144$ voxels ($\mathrm{P^C}$), respectively. Thus, tracer particles crossing control planes at $l_c = 0.1$ cm in $\mathrm{P^C}$ is roughly equivalent, in terms of the number of voxels traveled, to tracer particles crossing control planes at $l_c = 0.5$ cm in the first two rocks.

https://doi.org/10.5194/egusphere-2026-6561
Preprint. Discussion started: 5 November 2026
© Author(s) 2026. CC BY 4.0 License.

The parameter values used in the models $S_f(t)$ and $S(t)$ are shown in Table 3. A zoomed-in view of $S^N(t)$ for SW04 is shown in Figure 6, which more clearly compares the predictive performance of $S(t)$ and $S_f(t)$. When using $S_f(t)$ and $S(t)$ for fitting, we adopt the following criterion: the fitting parameters obtained from the best fit to the $S^N(t)$ curve with the largest l_c value are used to fit all $S^N(t)$ curves. This allows us to examine whether the transition can be described by the two models using a single set of parameters.

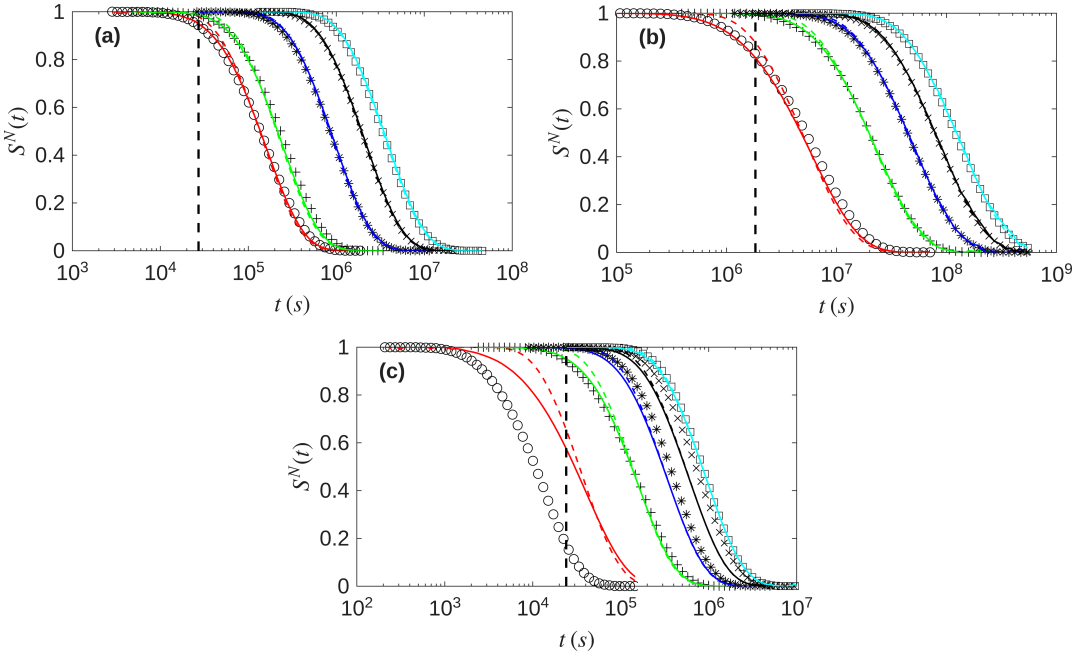


Figure 5. Computed survival probability curves, $S^N(t)$, from the particle-tracking simulations in the three porous media. (a) SW04; (b) P04; and (c) P^C. Different markers represent the computed $S^N(t)$ values for different control-plane pairs, l_c. The dashed and solid curves (shown in different colors) denote the best fits of the Fickian model, $S_f(t)$, and the truncated CTRW model, $S(t)$, respectively, to the $S^N(t)$ data for five different l_c values. The l_c values corresponding to each marker, the coefficients of determination (R^2), and the parameters used in the fits with $S(t)$ and $S_f(t)$ are shown in Table 3. The dashed black vertical lines in each subplot denote the transition time t_m in the model $S(t)$.

The transition from sub-diffusion to Fickian diffusion can be observed as the observation time or length scale l_c increases for diffusion in all three porous media. Sub-diffusion is reflected by the early arrivals and late-time tails of $S^N(t)$ compared with the $S_f(t)$ curves (e.g., the red solid curve and circle markers in Figure 5b). The truncated CTRW model, $S(t)$, better captures these two features of sub-diffusion, with a single set of parameters, as shown in Table 3. As the control-plane spacing l_c increases, the computed $S^N(t)$ curves progressively approach Fickian behavior, for which both $S(t)$ and $S_f(t)$ provide good predictions.

For P^C, the fits using either $S_f(t)$ or $S(t)$ fail to match the survival probabilities, except for the one with the largest l_c (square markers in Figure 5c). This digital sample is an artificial rock combining six different digital rocks, whose heterogeneity is

https://doi.org/10.5194/egusphere-2026-6561
Preprint. Discussion started: 5 November 2026
© Author(s) 2026. CC BY 4.0 License.

Table 3. The l_c values corresponding to the markers in each subplot of Figure 5, the parameters of the $S_f(t)$ and $S(t)$ models (shown as dashed and solid curves, respectively, in different colors), and their corresponding coefficients of determination (R^2).

(a): SW04

Marker	l_c	$S_f(t)$ parameters		$S(t)$ parameters			
		D_e	R^2	α	b	D	R^2
○	0.4	4.50×10^{-7}	0.9971	0.68	2.5×10^{-5}	1.19×10^{-2}	0.9996
+	0.5	4.50×10^{-7}	0.9962	0.68	2.5×10^{-5}	1.19×10^{-2}	0.9980
∗	1.0	4.50×10^{-7}	0.9996	0.68	2.5×10^{-5}	1.19×10^{-2}	0.9996
×	1.5	4.50×10^{-7}	0.9999	0.68	2.5×10^{-5}	1.19×10^{-2}	0.9999
□	2.0	4.50×10^{-7}	0.9999	0.68	2.5×10^{-5}	1.19×10^{-2}	0.9996

(b): P04

Marker	l_c	$S_f(t)$ parameters		$S(t)$ parameters			
		D_e	R^2	α	b	D	R^2
○	1.0	7.80×10^{-8}	0.9941	0.64	3.5×10^{-7}	1.40×10^{-1}	0.9976
+	2.0	7.80×10^{-8}	0.9988	0.64	3.5×10^{-7}	1.40×10^{-1}	0.9999
∗	3.0	7.80×10^{-8}	0.9994	0.64	3.5×10^{-7}	1.40×10^{-1}	0.9997
×	4.0	7.80×10^{-8}	0.9997	0.64	3.5×10^{-7}	1.40×10^{-1}	0.9996
□	5.0	7.80×10^{-8}	0.9999	0.64	3.5×10^{-7}	1.40×10^{-1}	0.9990

(c): $\mathrm{P^C}$

Marker	l_c	$S_f(t)$ parameters		$S(t)$ parameters			
		D_e	R^2	α	b	D	R^2
○	0.1	1.12×10^{-7}	0.6066	0.60	2.5×10^{-5}	2.70×10^{-3}	0.7405
+	0.2	1.12×10^{-7}	0.9938	0.60	2.5×10^{-5}	2.70×10^{-3}	0.9988
∗	0.3	1.12×10^{-7}	0.9919	0.60	2.5×10^{-5}	2.70×10^{-3}	0.9901
×	0.4	1.12×10^{-7}	0.9725	0.60	2.5×10^{-5}	2.70×10^{-3}	0.9703
□	0.5	1.12×10^{-7}	0.9999	0.60	2.5×10^{-5}	2.70×10^{-3}	0.9997

expected to be much stronger than that of the other two rocks. Tracer particles do not experience repeated porous structures. Thus, diffusion and the transition in such a rock cannot be described by either the CTRW model (with the specific truncated waiting-time distribution) introduced in this study or the Fickian model. A CTRW model with a different choice of the waiting time PDF may better match the simulations, but is beyond the scope of this study and can be investigated in the future. Nonetheless, the survival probabilities in Figure 5c show a transition from non-Fickian diffusion to Fickian diffusion, which is consistent with the MSD curve in Figure 4c.

In Figure 5, the $S^N(t)$ curves exhibit behavior similar to that observed in the theoretical CTRW-based survival probability curves in Figure 3: only those curves that begin to decay from one at times much larger than t_m (roughly more than two

https://doi.org/10.5194/egusphere-2026-6561
Preprint. Discussion started: 5 November 2026
© Author(s) 2026. CC BY 4.0 License.

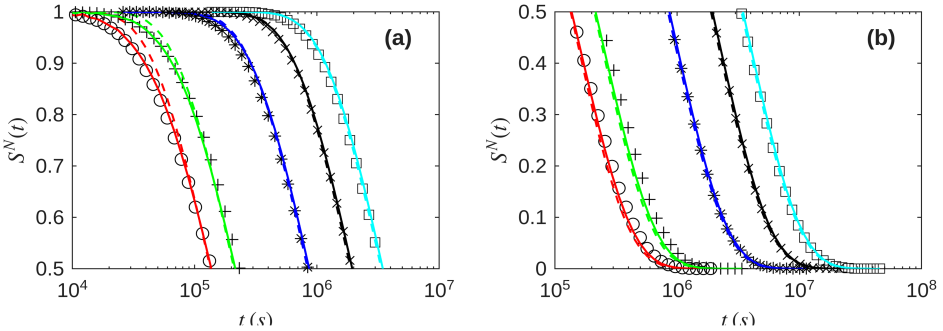


Figure 6. Zoomed-in view of Figure 5a. The markers, solid curves, and dashed curves have the same meanings as in Figure 5b. The relevant model parameters are shown in Table 3. Subplots (a) and (b) here show different temporal ranges of $S^N(t)$: (a) 0.5–1.0 and (b) 0–0.5.

orders of magnitude larger) can be well described by the Fickian model. Moreover, in Figure 4, the MSD gradually becomes linear after t_m, whereas in both Figures 3 and 5, the survival probability curves do not immediately approach Fickian behavior. This suggests that, although the observation time is already slightly larger than t_m, the survival probability is still affected by memory effects, and diffusion remains non-Fickian. This is consistent with previous work on dispersion (Dentz et al., 2004), which showed that transport can remain non-Fickian even at times well beyond the transition time.

From the values of l_c, we can roughly determine the length scale at which diffusion approaches the Fickian regime in each rock sample. For SW04, the $S^N(t)$ curve with $l_c = 1.5$ cm can be well fitted by $S_f(t)$, indicating that diffusion of tracer plumes becomes Fickian after they experience 1.5 repeated porous structures in either the $-x$ or x direction. This is shown by the x-shaped markers and the black solid curve in Figure 5a, as well as the corresponding value of R^2 in Table 3. For P04, the Fickian regime is attained at least when $l_c = 4.0$ cm, corresponding to four repeated domains. The substantial difference in the l_c values required to reach the Fickian regime suggests that stronger heterogeneity requires a longer distance for diffusion to become Fickian. This trend is further highlighted by diffusion in $\mathrm{P^C}$. This rock is constructed by combining six different rocks, and the Fickian regime is reached at $l_c = 0.5$ cm. Although this corresponds to approximately one domain, the domain itself consists of six different rocks and therefore represents a much longer and more heterogeneous porous structure. In real applications, if a rock formation consists of different layers, some of which have particularly low connectivity and strong heterogeneity, such as clay layers, Fickian diffusion may require very long distances to emerge or may be difficult to attain.

3.3 The transition to Fickian diffusion

Transitions to Fickian diffusion are observed numerically in all the rocks considered. This suggests that when a large rock contains repeated porous structures (e.g., P04 and SW04 under periodic boundary conditions), or when a highly heterogeneous rock ($\mathrm{P^C}$) is observed over a sufficiently long length scale (comparable to the domain size L_m here), diffusion eventually evolves toward Fickian behavior.

The causes of the transition to Fickian diffusion can be explained qualitatively as follows. At sufficiently long time and distance scales, tracers sample a large number of diffusion events, progressively averaging out the trapping and memory effects

https://doi.org/10.5194/egusphere-2026-6561
Preprint. Discussion started: 5 November 2026
© Author(s) 2026. CC BY 4.0 License.



associated with locally poorly connected pore structures. In addition, extremely long trapping events are suppressed by the finite physical scales of the pore structure and the finite duration of tracer immobilization (Rajyaguru et al., 2025). Consequently, the transport gradually approaches an effectively Fickian regime, although the effective diffusion coefficient may remain reduced due to continuing short-time immobilization events (as indicated by the comparison between D_m in Equation (1) and D_e in Table 3).

3.4 Implications of sub-diffusion

The applicability of the Fickian model depends on the relationship between the observation time and the characteristic time scale t_m. If diffusion in a porous medium eventually evolves from sub-diffusion to Fickian diffusion, a classical Fickian model may provide an adequate description of the long-time asymptotic diffusive transport. However, it cannot capture the sub-diffusive dynamics that occur prior to the transition.

In reality, diffusion of conservative solute tracers in large-scale porous rocks may exhibit sub-diffusion before eventually approaching the Fickian regime. Using a purely Fickian model as the governing equation assumes that this behavior is absent: this can lead to inaccurate predictions of early-time diffusion processes, breakthrough curves, and first-passage statistics.

Early time is a relative concept here; it may refer not only to hours or days but also to months or even years. Note that previous experiments have observed sub-diffusion over 70 days in porous rocks (Rajyaguru et al., 2025). The implications of sub-diffusion can be illustrated using an artificial example relevant to diffusion in SW04. Suppose that diffusion in an real infinite rock follows the CTRW model given by Equation (7), with $\alpha = 0.68$, $b = 2.5 \times 10^{-5}$, and $D = 1.19 \times 10^{-2}$ (Table 3). A Fickian model with $D_e = 4.50 \times 10^{-7}$ is used for comparison, with the Green's function in Equation (11) employed to calculate the Fickian Breakthrough curves (BTCs).

A sampling location at $x_s = 0.2$ is selected to measure the BTCs, $B(x,t)$, as shown in Figure 7. The "real" BTC (described by the truncated CTRW model) exhibits earlier arrivals than that predicted by the Fickian model, while the tails of the two BTCs gradually merge because, at sufficiently long times, the truncated CTRW model asymptotically approaches the Fickian regime.

Figure 7 suggests that using a Fickian model could underestimate, for example, the concentration of a diffusive pollutant plume at an observation location during early times. The relative error (E_{early}) associated with this early-time underestimation can be quantified in this example as

$$E_{\text{early}} = \frac{B_{\text{CTRW}} - B_{\text{F}}}{B_{\text{CTRW}}}, \tag{12}$$

at the early time $t = 3 \times 10^3$, where B_{CTRW} and B_{F} are the concentrations observed at location x_s and time $t = 3 \times 10^3$, as predicted by the truncated CTRW and Fickian models, respectively. The resulting value, $E_{\text{early}} = 97.15\%$, indicates that the Fickian model substantially underestimates the early-time BTC.

We note again that if there is an infinite hierarchy of trapping scales, or if the pore structure is exactly at the percolation threshold, the transition theoretically does not exist. Simulations with periodic boundary conditions in lattice percolation net-

https://doi.org/10.5194/egusphere-2026-6561
Preprint. Discussion started: 5 November 2026
© Author(s) 2026. CC BY 4.0 License.

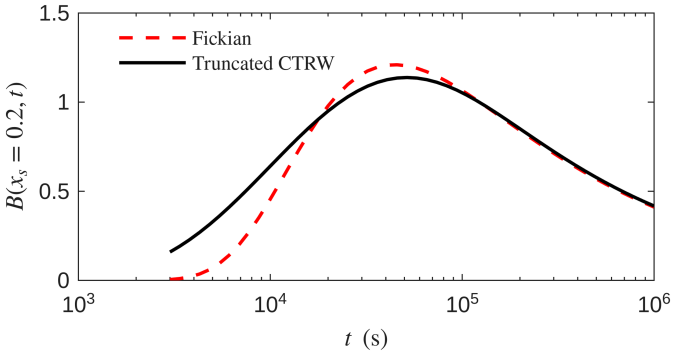


Figure 7. Breakthrough curves for the artificial example predicted by the truncated CTRW and Fickian models.

works near the percolation threshold exhibit non-Fickian diffusion over all time scales (Mardoukhi et al., 2015). Thus, there is still a non-zero possibility that sub-diffusion can persist indefinitely

This work also suggests that using diffusion results obtained from small samples to infer larger-scale diffusion behavior can be problematic. First, pre-asymptotic diffusion can be non-Fickian when the time/length scale is not sufficiently large, as indicated by the early-time mismatch between the Fickian and truncated CTRW models in Figure 7. Second, even when a Fickian signature is observed, the effective diffusion coefficient D_e can remain scale-dependent. In Figure 8, the $S^N(t)$ curves are fitted independently using the Fickian model $S_f(t)$, without fixing D_e (note that in Figure 5c, the fitted D_e value obtained from the $S^N(t)$ curve with the largest l_c is used to fit all curves). The D_e values obtained from the best fits are reported in Table 4. Based on both the visual agreement and the reported R^2 values, the third curve ($l_c = 0.3$ cm) already exhibits a nearly Fickian signature. However, the fitted effective diffusion coefficients D_e reported in Table 4 vary considerably with l_c. Therefore, even when the effective diffusion behavior exhibits a Fickian-like signature, as indicated by the survival probability curves, the diffusion cannot necessarily be characterized by a single scale-independent D_e. Such scale dependence may be particularly relevant in heterogeneous porous media and should be considered when extrapolating diffusion behavior across length scales.

Table 4. The l_c values corresponding to the markers in Figure 8, the parameters of the $S_f(t)$ models (shown as dashed curves in different colors), and the corresponding coefficients of determination (R^2).

Marker	l_c	D_e	R^2
○	0.1	3.67×10^{-7}	0.9969
+	0.2	1.16×10^{-7}	0.9940
*	0.3	9.54×10^{-8}	0.9998
×	0.4	8.60×10^{-8}	0.9998
□	0.5	1.12×10^{-7}	0.9999

https://doi.org/10.5194/egusphere-2026-6561
Preprint. Discussion started: 5 November 2026
© Author(s) 2026. CC BY 4.0 License.

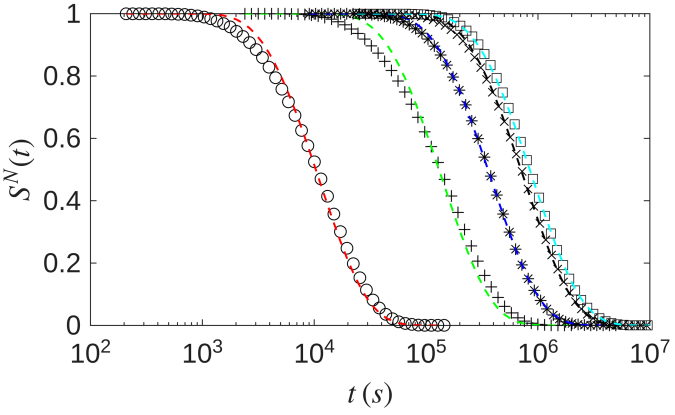


Figure 8. Computed survival probability curves, $S^N(t)$, from the particle-tracking simulations in $\mathrm{P^C}$. The markers denote the $S^N(t)$ values, which are the same as those shown in Figure 5c. The dashed curves denote the best fits obtained using the Fickian model $S_f(t)$ without fixing the D_e values, which are reported in Table 4.

4 Conclusions

In principle, diffusion of conservative solute tracers in porous rocks can transition from sub-diffusion to Fickian diffusion over increasing length and/or time scales. Using a truncated CTRW model and particle-tracking simulations with periodic boundary conditions, we demonstrate such transitions both analytically and numerically. The transition is described by a characteristic time beyond which diffusion approaches the Fickian regime.

The classical Fickian model neglects the early-time sub-diffusion, which in large-scale diffusion modeling may lead to inaccurate predictions of early-time diffusive transport processes of e.g., contaminants in the subsurface. The truncated CTRW model provides an alternative framework for capturing this sub-diffusive behavior. For natural porous rocks with an infinite hierarchy of trapping scales or pore structures near the percolation threshold, sub-diffusion may persist over all time scales. Whether such behavior occurs in natural porous rocks remains an open question and warrants further investigation.

Code availability. The data supporting the findings of this study were generated from numerical simulations performed using an open-sourced computational codes (Yin, 2026).

Data availability. The porous media digital samples are obtained from open data sources (Eduardo Menezes dos Anjos et al., 2024). The data generated by the simulation code are available in a Mendeley Data repository (Yin, 2026).

https://doi.org/10.5194/egusphere-2026-6561
Preprint. Discussion started: 5 November 2026
© Author(s) 2026. CC BY 4.0 License.

Appendix A: Auxiliary functions in the analytical solution of concentration profiles

The auxiliary functions appearing in Equation (7) are defined below:

$$\Phi(\omega,x)=\frac{\sqrt{r_2(\omega)}}{\omega}\exp\left[-\frac{|x|}{\sqrt{Db^{\alpha}}}\sqrt{r_2(\omega)}\cos\left(\frac{\theta_2(\omega)}{2}\right)\right], \tag{A1}$$

and

$$\theta(\omega,x)=\frac{\theta_2(\omega)-\pi}{2}-\frac{|x|}{\sqrt{Db^{\alpha}}}\sqrt{r_2(\omega)}\sin\left(\frac{\theta_2(\omega)}{2}\right), \tag{A2}$$

with

$$r_1(\omega)=\sqrt{\omega^2+b^2}, \tag{A3}$$

$$\theta_1(\omega)=\arccos\left(\frac{b}{r_1(\omega)}\right), \tag{A4}$$

$$r_2(\omega)=\sqrt{[r_1^{\alpha}(\omega)\cos(\alpha\theta_1(\omega))-b^{\alpha}]^2+r_1^{2\alpha}(\omega)\sin^2(\alpha\theta_1(\omega))}, \tag{A5}$$

and

$$\theta_2(\omega)=\arccos\left(\frac{r_1^{\alpha}(\omega)\cos(\alpha\theta_1(\omega))-b^{\alpha}}{r_2(\omega)}\right). \tag{A6}$$

Appendix B: Auxiliary functions in the survival probability model

The auxiliary functions in Equation (10) are defined below:

$$A(\omega)=\frac{\sqrt{r_2}}{\omega}, \tag{B1}$$

$$\phi(\omega)=\frac{\theta_2-\pi}{2}, \tag{B2}$$

$$\begin{aligned}\mathcal{I}_c^{(+)}-\mathcal{I}_c^{(-)}=&\frac{2\lambda\left(\cos(L\mu)-2\cos\left(\frac{L\mu}{2}\right)\cosh\left(\frac{L\lambda}{2}\right)+\cosh(L\lambda)\right)}{(\lambda^2+\mu^2)\left(\cos(L\mu)+\cosh(L\lambda)\right)}\\&+\frac{4\mu\sin\left(\frac{L\mu}{2}\right)\sinh\left(\frac{L\lambda}{2}\right)}{(\lambda^2+\mu^2)\left(\cos(L\mu)+\cosh(L\lambda)\right)},\end{aligned} \tag{B3}$$

https://doi.org/10.5194/egusphere-2026-6561
Preprint. Discussion started: 5 November 2026
© Author(s) 2026. CC BY 4.0 License.

and

$$\mathcal{I}_s^{(+)} - \mathcal{I}_s^{(-)} = \frac{2\mu\left(\cos(L\mu) - 2\cos\left(\frac{L\mu}{2}\right)\cosh\left(\frac{L\lambda}{2}\right) + \cosh(L\lambda)\right)}{(\lambda^2+\mu^2)\left(\cos(L\mu)+\cosh(L\lambda)\right)} - \frac{4\lambda\sin\left(\frac{L\mu}{2}\right)\sinh\left(\frac{L\lambda}{2}\right)}{(\lambda^2+\mu^2)\left(\cos(L\mu)+\cosh(L\lambda)\right)}, \tag{B4}$$

where

$$\mu(\omega) = \frac{\sqrt{r_2}}{\sqrt{Db^\alpha}}\sin\left(\frac{\theta_2}{2}\right), \tag{B5}$$

and

$$\lambda(\omega) = \frac{\sqrt{r_2}}{\sqrt{Db^\alpha}}\cos\left(\frac{\theta_2}{2}\right). \tag{B6}$$

Author contributions. Conceptualization and supervision: T. Y. and B. B.; Design and methodology: T. Y. and B. B.; Data analysis: T. Y.; Data curation: T. Y.; Writing-original draft preparation: T. Y.; Writing-review and editing: T. Y. and B. B.

Competing interests. At least one of the (co-)authors is a member of the editorial board of Hydrology and Earth System Sciences.

Acknowledgements. T.Y. is grateful to the Azrieli Foundation for support through the Azrieli International Postdoctoral Fellowship. B.B. gratefully acknowledges support through the ViTamins project, funded by the Volkswagen Foundation (grant no. AZ 9B192). B.B. holds the Sam Zuckerberg Professorial Chair in Hydrology.

https://doi.org/10.5194/egusphere-2026-6561
Preprint. Discussion started: 5 November 2026
© Author(s) 2026. CC BY 4.0 License.

References

Aarão Reis, F. and Di Caprio, D.: Crossover from anomalous to normal diffusion in porous media, Physical Review E, 89, 062 126, https://doi.org/10.1103/PhysRevE.89.062126, 2014.

Arbabi, S. and Sahimi, M.: The Transition from Darcy to Nonlinear Flow in Heterogeneous Porous Media: I—Single-Phase Flow, Transport in Porous Media, 151, 795–812, https://doi.org/10.1007/s11242-024-02070-3, 2024.

Berkowitz, B.: HESS Opinions: Chemical transport modeling in subsurface hydrological systems–Space, time, and the "holy grail" of "upscaling", Hydrology and Earth System Sciences, 2021, 1–31, https://doi.org/10.5194/hess-26-2161-2022, 2021.

Berkowitz, B. and Scher, H.: Exploring the nature of non-Fickian transport in laboratory experiments, Advances in Water Resources, 32, 750–755, https://www.sciencedirect.com/science/article/pii/S0309170808000900, 2009.

Bijeljic, B., Mostaghimi, P., and Blunt, M. J.: Signature of non-Fickian solute transport in complex heterogeneous porous media, Physical review letters, 107, 204 502, https://doi.org/10.1103/PhysRevLett.107.204502, 2011.

Chen, S., Serkh, K., and Bremer, J.: On the adaptive Levin method, Numerische Mathematik, 156, 1927–1985, https://doi.org/10.1007/s00211-024-01443-6, 2024.

Clarke, D. A., Dolamore, F., Fee, C. J., Galvosas, P., and Holland, D. J.: Investigation of flow through triply periodic minimal surface-structured porous media using MRI and CFD, Chemical Engineering Science, 231, 116 264, https://doi.org/10.1016/j.ces.2020.116264, 2021.

Cohen, M. and Berkowitz, B.: Exploring asymptotically-Fickian chemical transport in porous media, Journal of Contaminant Hydrology, 278, 104 884, https://doi.org/10.1016/j.jconhyd.2026.104884, 2026.

Delay, F., Porel, G., and Sardini, P.: Modelling diffusion in a heterogeneous rock matrix with a time-domain Lagrangian method and an inversion procedure, Comptes Rendus Geoscience, 334, 967–973, https://doi.org/10.1016/S1631-0713(02)01835-7, 2002.

Deng, J., Sharma, R. P., Szymczak, P., and Kang, P. K.: Anomalous transport in dissolving porous media: Transitions between Fickian and non-Fickian regimes, Geophysical Research Letters, 52, e2025GL115 940, https://doi.org/10.1029/2025GL115940, 2025.

Dentz, M., Cortis, A., Scher, H., and Berkowitz, B.: Time behavior of solute transport in heterogeneous media: transition from anomalous to normal transport, Advances in Water Resources, 27, 155–173, https://doi.org/10.1016/j.advwatres.2003.11.002, 2004.

Dentz, M., Gouze, P., Russian, A., Dweik, J., and Delay, F.: Diffusion and trapping in heterogeneous media: An inhomogeneous continuous time random walk approach, Advances in Water Resources, 49, 13–22, https://doi.org/10.1016/j.advwatres.2012.07.015, 2012.

Eduardo Menezes dos Anjos, C., Medeiros, L., Surmas, R., Neta, A., Evsukoff, A., and Vargas, J.: 16 Brazilian pre-salt carbonates: multi-resolution micro-CT images, https://doi.org/10.17612/XR50-S717, 2024.

Fa, K. S.: Continuous-time random walk: Crossover from anomalous regime to normal regime, Physical Review E, 82, 012 101, https://doi.org/10.1103/PhysRevE.82.012101, 2010.

Fa, K. S. and Wang, K.: Integrodifferential diffusion equation for continuous-time random walk, Physical Review E, 81, 011 126, https://doi.org/10.1103/PhysRevE.81.011126, 2010.

Fetter, C. W., Boving, T., and Kreamer, D.: Contaminant Hydrogeology, Waveland Press, 2017.

García-Gutiérrez, M., Cormenzana, J., Missana, T., Mingarro, M., and Martin, P.: Large-scale laboratory diffusion experiments in clay rocks, Physics and Chemistry of the Earth, Parts A/B/C, 31, 523–530, https://doi.org/10.1016/j.pce.2006.04.004, 2006.

Garcia-Gutierrez, M., Mingarro, M., Morejon, J., Alonso, U., and Missana, T.: Analysis of the role of water saturation degree in HTO, 36Cl, and 75Se diffusion in sedimentary rock, Minerals, 13, 593, https://doi.org/10.3390/min13050593, 2023.

https://doi.org/10.5194/egusphere-2026-6561
Preprint. Discussion started: 5 November 2026
© Author(s) 2026. CC BY 4.0 License.

Gouze, P., Melean, Y., Le Borgne, T., Dentz, M., and Carrera, J.: Non-Fickian dispersion in porous media explained by heterogeneous microscale matrix diffusion, Water Resources Research, 44, https://doi.org/10.1029/2007WR006690, 2008.

Grigaliuniene, D., Balcius, P., Jacques, D., and Poskas, P.: Assessment of intermediate level radioactive waste disposal cell evolution in granitic host rock applying abstracted reactive transport models, Environmental earth sciences, 83, 575, https://doi.org/10.1007/s12665-024-11885-8, 2024.

Koch, D. L. and Brady, J. F.: Anomalous diffusion in heterogeneous porous media, The Physics of fluids, 31, 965–973, https://doi.org/10.1063/1.866716, 1988.

Mardoukhi, Y., Jeon, J.-H., and Metzler, R.: Geometry controlled anomalous diffusion in random fractal geometries: looking beyond the infinite cluster, Physical Chemistry Chemical Physics, 17, 30 134–30 147, https://doi.org/10.1039/c5cp03548a, 2015.

Metzler, R. and Klafter, J.: Boundary value problems for fractional diffusion equations, Physica A: Statistical Mechanics and its Applications, 278, 107–125, https://doi.org/10.1016/S0378-4371(99)00503-8, 2000.

Metzler, R., Rajyaguru, A., and Berkowitz, B.: Modelling anomalous diffusion in semi-infinite disordered systems and porous media, New journal of physics, 24, 123 004, https://doi.org/10.1088/1367-2630/aca70c, 2022.

Montroll, E. W. and Weiss, G. H.: Random walks on lattices. II, Journal of Mathematical Physics, 6, 167–181, https://doi.org/10.1063/1.1704269, 1965.

Nasir, O., Fall, M., and Evgin, E.: A simulator for modeling of porosity and permeability changes in near field sedimentary host rocks for nuclear waste under climate change influences, Tunnelling and underground space technology, 42, 122–135, https://doi.org/10.1016/j.tust.2014.02.010, 2014.

Pacheco-Pozo, A. and Sokolov, I. M.: Random walks in correlated diffusivity landscapes, The European Physical Journal B, 96, 152, https://doi.org/10.1140/epjb/s10051-023-00621-z, 2023.

Rajyaguru, A., Metzler, R., Dror, I., Grolimund, D., and Berkowitz, B.: Diffusion in porous rock is anomalous, Environmental Science & Technology, 58, 8946–8954, https://doi.org/10.1021/acs.est.4c01386, 2024.

Rajyaguru, A., Metzler, R., Cherstvy, A. G., and Berkowitz, B.: Quantifying anomalous chemical diffusion through disordered porous rock materials, Physical Chemistry Chemical Physics, 27, 9056–9067, https://doi.org/10.1039/d5cp00654f, 2025.

Redner, S.: A guide to first-passage processes, Cambridge university press, 2001.

Redner, S.: A first look at first-passage processes, Physica A, 631, 128 545, https://doi.org/10.1016/j.physa.2023.128545, 2023.

Regner, B. M., Vučinić, D., Domnisoru, C., Bartol, T. M., Hetzer, M. W., Tartakovsky, D. M., and Sejnowski, T. J.: Anomalous diffusion of single particles in cytoplasm, Biophysical journal, 104, 1652–1660, https://doi.org/10.1016/j.bpj.2013.01.049, 2013.

Sahimi, M.: Flow and transport in porous media and fractured rock: from classical methods to modern approaches, John Wiley & Sons, 2011.

Soler, J. M., Neretnieks, I., Moreno, L., Liu, L., Meng, S., Svensson, U., Iraola, A., Ebrahimi, H., Trinchero, P., Molinero, J., et al.: Predictive modeling of a simple field matrix diffusion experiment addressing radionuclide transport in fractured rock. Is it so straightforward?, Nuclear Technology, 208, 1059–1073, https://doi.org/10.1080/00295450.2021.1988822, 2022.

Sowiżdżał, A., Machowski, G., Krzyżak, A., Puskarczyk, E., Krakowska-Madejska, P., and Chmielowska, A.: Petrophysical evaluation of the Lower Permian formation as a potential reservoir for CO2-EGS–Case study from NW Poland, Journal of Cleaner Production, 379, 134 768, https://doi.org/10.1016/j.jclepro.2022.134768, 2022.

Stauffer, D. and Aharony, A.: Introduction to percolation theory, taylor & Francis, 2018.

Szymczak, P. and Ladd, A.: Boundary conditions for stochastic solutions of the convection-diffusion equation, Physical Review E, 68, 036 704, https://doi.org/10.1103/PhysRevE.68.036704, 2003.

https://doi.org/10.5194/egusphere-2026-6561
Preprint. Discussion started: 5 November 2026
© Author(s) 2026. CC BY 4.0 License.



Tartakovsky, D. M. and Dentz, M.: Diffusion in porous media: phenomena and mechanisms, Transport in Porous Media, 130, 105–127, https://doi.org/10.1007/s11242-019-01262-6, 2019.

Vidal, A. D., Neta, A. P. M., de Castro Vargas Fernandes, J., Medeiros, L. C., Dos Anjos, C. E. M., Surmas, R., and Evsukoff, A. G.: Multi-resolution X-ray micro-computed tomography images of carbonate rocks from Brazilian pre-salt, Scientific Data, 11, 1361, https://doi.org/10.1038/s41597-024-04198-9, 2024.

Wersin, P., Van Loon, L., Soler, J., Yllera, A., Eikenberg, J., Gimmi, T., Hernán, P., and Boisson, J.-Y.: Long-term diffusion experiment at Mont Terri: first results from field and laboratory data, Applied Clay Science, 26, 123–135, https://doi.org/10.1016/j.clay.2003.09.007, 2004.

Wu, J., Chen, Q., Jiang, J., Chatzigeorgiou, G., and Meraghni, F.: Adaptive deep homogenization theory for periodic heterogeneous materials, Composite Structures, 340, 118 171, https://doi.org/10.1016/j.compstruct.2024.118171, 2024.

Yin, T.: Codes and datasets for the manuscript "From Sub-Diffusion to Fickian Diffusion of Conservative Solute Tracers in Porous Rocks", https://doi.org/0.17632/xydgpfxjtn.1, Mendeley Data, V1, 2026.

Yin, T. and Berkowitz, B.: Structural controls on non-Fickian and Fickian chemical tracer diffusion in porous media, manuscript under review, 2026.

Yin, T., Man, T., Zhang, P., and Galindo-Torres, S. A.: Péclet-number-dependent longitudinal dispersion in discrete fracture networks, Water Resources Research, 60, e2024WR038 437, https://doi.org/10.1029/2024WR038437, 2024.

Yin, T., Man, T., Zhang, P., and Galindo-Torres, S. A.: GPU-accelerated simulation of steady-state flow and particle transport in discrete fracture networks, Applied Computing and Geosciences, p. 100284, https://doi.org/10.1016/j.acags.2025.100284, 2025.

Zhang, P., Zhao, Y., Galindo-Torres, S., Chen, Y., Tang, H., Jin, G., Scheuermann, A., and Li, L.: Random walk discrete element lattice boltzmann model for scalar transport in fluid and particle flows with strict scalar mass conservation, International Journal of Heat and Mass Transfer, 187, 122 577, https://doi.org/10.1016/j.ijheatmasstransfer.2022.122577, 2022.

Zhokh, A. and Strizhak, P.: Crossover between Fickian and non-Fickian diffusion in a system with hierarchy, Microporous and Mesoporous Materials, 282, 22–28, https://doi.org/10.1016/j.micromeso.2019.03.016, 2019.